Spectroscopy of highly-charged Sn ions for extreme ultraviolet nanolithography

Torretti, F.

2019

document version
Publisher's PDF, also known as Version of record

Introduction

> There is nothing like professionalism. It is what makes humanity worth preserving.
>
> Jerry Seinfeld

Since the invention of the transistor [1, 2] and its applications in integrated circuits [3, 4], semiconductor devices have become ubiquitous in our everyday lives. The generic term "semiconductor devices" casts a very wide net, covering small and low-power microprocessors found in ultra-thin laptops, smartphones, smartwatches and other wearables; flash memory like NAND Flash or V-NAND; random-access memory, i.e. DRAM or SRAM; and reaching all the way to server-grade equipment for cloud computing infrastructures and data centers. Undoubtedly, these devices affect society in a deep manner and drastically improve our lives. Moreover, the semiconductor industry is a strong player in the world economy, having grown in 2017 to be a €360 billion industry [5] while also powering the much larger economy of the products related to integrated circuits.

Improvements in the design of integrated circuits can be attributed, amongst other factors, to the miniaturization of micro-electronic components enabling, for example, a greater number of transistors per unit area in a microprocessor. It was first Gordon Moore, co-founder of Intel, who predicted in 1965 that the number of components in integrated circuits would double every year [6]. Ten years later, once this empirical law was adjusted to doubling every two years [7], it became a point of reference for chipmakers and the semiconductor industry. Thanks to the effort of industrial partners to co-ordinate their activities through the bi-yearly release of a research road map [8], Moore's law, as it became known, has been followed for the past five decades [9].

The shrinking of components, and the faultlessness of Moore's law, is directly driven by improvements in the industrial process for the production of

integrated circuits: photolithography [10]. In its simplest form, the photolithographic process consists of a light source projecting a pattern onto a silicon wafer covered with a medium (photoresist) which reacts with the light in such a way that further processing of the wafer will imprint the pattern on the semiconductor. It is quite intuitive to understand that the performance of a photolithograpic system, in terms of the size of the imprinted features, is directly linked to the optical properties of the light source and of its optical system used to project the pattern onto the wafer. The minimum resolvable feature, most commonly referred to as the critical dimension (CD), is determined by the following equation:

$$\mathrm{CD} = k_1 \cdot \frac{\lambda}{\mathrm{NA}}, \tag{I.1}$$

where k_1 is a constant related to the specifics of the lithographic process, λ is the photon wavelength, and NA is the numerical aperture of the optical system. In the past few decades, the vast majority of improvements in CD came from reduction of the exposure wavelength or increases in the numerical aperture. Figure I.1 illustrates the development of photolithography machines from the Dutch company ASML [11] in the last 35 years. The miniaturization of the critical dimension over these years is clearly shown to be driven by the factors discussed above. The CD presented here refers to the minimum dimension achievable in a single exposure. In reality, thanks to the adoption of advanced techniques such as multiple-patterning [12], the final critical dimension can be made much smaller than the resolution limit. In fact, features down to 20 nm have been produced with 193 nm illumination. This, however, comes at great economic costs due to the multiple illumination and development cycles required for a single wafer.

In order to address these increased costs and to allow for smaller CD in a single wafer exposure, the industry has spent the last 20 years preparing for the paradigm shift of extreme ultraviolet (EUV) lithography [14, 15], in which the exposure wavelength of choice is 13.5 nm. In fact, going from 193 nm to 13.5 nm means that drastic changes need to be enacted in the entirety of the lithographic machine. First of all, such short-wavelength radiation is strongly absorbed by the vast majority of media, and therefore the entire process must be carried in vacuum. For the very same reason, lenses cannot be employed in the optical system which must be re-designed using only reflective elements. Even in the case of mirrors, special coatings must be used to ensure that the radiation will in fact be reflected from the surface. Fortunately, it is possible to manufacture multi-layer mirrors (MLMs) with the ability to reflect 13.5 nm photons [16]: by alternating few-nm-thick layers of molybdenum and silicon, the incoming radiation will interfere within these layers and be reflected, with maximum peak

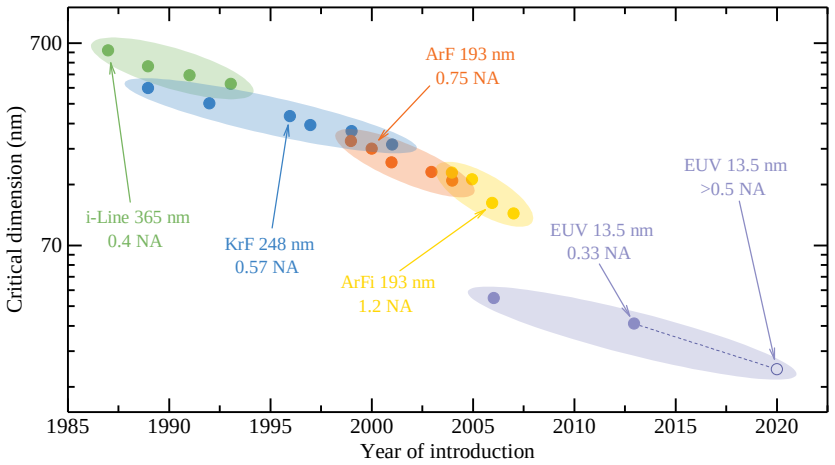

FIGURE I.1 Miniaturization of the single-exposure critical dimension in the past 35 years for ASML lithography machines. The various exposure wavelengths and the respective light sources are indicated by the different colors: in green, 365 nm i-Line (emission from a Hg lamp filtered at the desired wavelength); in blue, 248 nm KrF excimer laser; in orange, 193 nm ArF excimer laser; in yellow, 193 nm ArFi which uses the same ArF laser but with the wafer immersed in water allowing for a NA above 1; in violet, 13.5 nm generated by Sn laser-produced-plasma (see main text). Adapted from Ref. [13].

reflectivities of approximately 70 % centered at 13.5 nm with a 2 % bandwidth. It is now only a matter of producing the short-wavelength photons.

In industrial applications, the EUV photons are generated by irradiating micrometer-sized droplets of molten Sn with an intense laser pulse [17, 18]. High-power 10.6-μm-wavelength CO_2 lasers are currently employed, being able to produce the necessary laser intensities, in the order of $10^{10}\,\mathrm{W/cm^2}$, which allow for the creation of a hot, dense Sn plasma. To improve the conversion of laser light into EUV photons, a two-step process is adopted in which a low intensity laser *prepulse* first deforms the spherical droplet into a flat, disk-like target [19, 20]. Following this deformation, a higher intensity *main pulse* irradiates the target generating a plasma having temperatures and densities in the range 20–40 eV and 10^{18}–$10^{19}\,e/\mathrm{cm^3}$, respectively [21]. This process is repeated with frequencies up to 50 kHz. These sources are currently able to convert laser light into EUV with an efficiency of 5–6 %, allowing for the production of 250 W of EUV power in the 2 % bandwidth delivered by the source to the lithogra-

phy scanner. In the pursuit of producing more and more EUV photons, there exists a line of research into 1-μm-wavelength-driven sources [22]. Solid-state YAG lasers offer many technological advantages over CO_2 gas lasers, such as more compact size, improved wall-plug efficiencies, and better temporal pulse-shaping capabilities. The applicability of these solid-state lasers in EUV sources have been studied both for the prepulse [23–26] and the main pulse [27]. The shorter laser-wavelength introduces some interesting changes at the physical level: 1-μm radiation, in fact, is capable of traveling into plasma regions one hundred times denser than in the CO_2-laser case. This density increase has several consequences, e.g. increasing the laser absorption by the plasma to near-unity values. More importantly, when looking at main pulse YAG applications, EUV photons are now being produced at higher plasma densities. These conditions are such that now, in comparison with CO_2-produced-plasma, the emitted radiation suffers from self-absorption due to the surrounding ions. Absorption is well-known to cause broadening of the spectral emission features [28, 29], to some extent re-distributing energy across the spectral range outside the bandwidth accepted by MLMs. This lowers the overall conversion efficiency of laser light into EUV photons, with the record-high number recently recorded of 3.2 % [27].

The peculiar aptness of Sn laser-produced plasma to generate EUV photons is ultimately connected to the fortuitous atomic structure of the Sn ions at play in these processes [30]. For the plasma conditions outlined in the previous paragraph, the Sn^{10+}–Sn^{14+} ions are produced. Their atomic structures are determined by their ground configurations in the form $4p^6\,4d^m$, with $m = 4 - 0$. It is fairly well established that Sn ions exhibit an interesting behavior regarding their electric dipole excitations $4p \rightarrow 4d$ and $4d \rightarrow 4f$, resulting in the strongly-mixed excited configurations $4p^5\,4d^{m+1}$ and $4p^6\,4d^{m-1}\,4f$, respectively. These excited configuration and their respective levels have very similar excitation energies, and therefore strong configuration-interaction effects are observed [31], which cause a re-distribution of the transitions oscillator strengths to favor, in the Sn case, the short-wavelength transitions around 13.5 nm [30]. The coupling of high-angular-momentum electrons generates a considerable amount of states, which in turn allows for several thousands radiative de-excitation channels towards the ground levels of the ions through strong electric dipole transitions [32–36]. Moreover, these transition energies remains fairly constant across the isonuclear sequence Sn^{10+}–Sn^{14+} [37] as seen in figure I.2, which illustrates these properties using the emission spectra of Sn ions obtained in an ion trap. Therefore, Sn ions are excellent, bright radiators of 13.5 nm photons, with their serendipitous atomic structure being, for the most part, responsible for Sn becoming the element of choice for the lithography industry, above other EUV radiators such as Xe or Li.

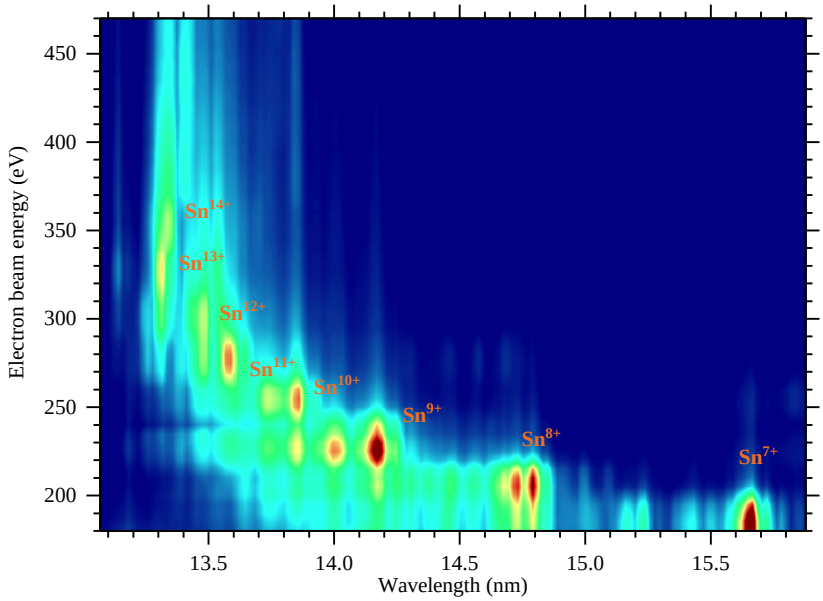

FIGURE I.2 Fluorescence of Sn ions measured at an electron beam ion trap at the Max Planck institute for Nuclear Physics in Heidelberg. The electron beam energy, shown on the y-axis, determines the ionization staged produced in the ion trap (see chapters 1 and 2 for more details). The emission here presented is from transitions to the ground configurations of these ions from the excited states $4p^5\,4d^{m+1}$ and $4p^6\,4d^{m-1}\,4f$, where $m = 7 - 0$ for Sn^{7+}–Sn^{14+}.

Thesis outline and summary

This thesis aims to further the understanding of the Sn ions responsible for emission of 13.5 nm radiation in laser-produced-plasma EUV sources for the nanolithographic industry. It collects the work performed at the Advanced Research Center for Nanolithography (ARCNL) in Amsterdam, in the EUV Plasma Processes group, and partly at the Max Planck Institute for Nuclear Physics in Heidelberg, Germany.

Chapter 1 and chapter 2 present the results of optical spectroscopy performed in an electron beam ion trap at the Max Planck institute for Nuclear Physics in Heidelberg, Germany. The ions Sn^{7+}–Sn^{14+} were created in the magnetic field of the ion trap using a monochromatic high-energy electron beam. The electrons ionize and excite the Sn ions through ion-electron collisions. Due

to the low collision frequency, the excited states are allowed to cascade towards their ground states and even transitions with very low transition probabilities can be observed. In these chapters, the magnetic dipole transitions within the ground-state manifolds of the studied ions were measured in the 200–700 nm range. These transitions were identified using three different atomic structure codes: the semi-empirical Cowan code, based on the semi-relativistic Hartree-Fock approach; the ab initio TRAFS-3C (Tel Aviv relativistic atomic FSCC code), based on Fock space coupled cluster; and the ab initio AMBiT code, based on the configuration-interaction + many-body perturbation theory. The work in these chapters presents two important results: firstly, the capabilities of these ab initio codes are such that even the complicated open-$4d$-shell atomic structure of the Sn ions investigated can be calculated with an unprecedented level of accuracy, which yet is still not sufficient to perform line-assignments without the help of semi-empirical Cowan code calculations; secondly, the level assignments performed have re-evaluated the fine structure of these ions, highlighting inaccuracies in previous, ground-laying works which will have to be revised.

Spectroscopy remains the main focus of chapter 3, but in the extreme ultraviolet regime. The light source used is a custom-built, droplet-based, laser-produced-plasma Sn EUV source built at ARCNL. The micrometer-sized droplets were irradiated by a high-energy, high-intensity 1-µm-wavelength laser pulse. The emission between 6 nm and 17 nm was recorded. This chapter focuses on the so-called "out-of-band" radiation, i.e. radiation outside the 2 % wavelength bandwidth, in order to unravel the various charge state contributions which are unresolved around 13.5 nm. The emission features found between 6 nm and 12 nm were investigated using the flexible atomic code (FAC). The investigation showed that a previous publication examining the same transitions had neglected what the present study has identified as the main contributor to the spectrum. The atomic structure calculation successfully associated all emission features observed to electric dipole transitions from excited states towards the ground-state manifold.

The results on the out-of-band radiation are applied in chapter 4 in order to analyze EUV spectra obtained at an industrial ASML light source. During the experiments, performed in the EUV cleanroom at ASML Veldhoven, the 10-µm-wavelength drive laser beam-spot was changed through manipulation of the beam optics. Changing the size of the laser beam, while keeping laser energy and duration constant, results in intensity changes. In laser-produced-plasma physics, laser intensity is the principal quantity setting the plasma temperature. By fitting the atomic structure calculations presented in chapter 3 to the experimental data, the contributions of the charge states Sn^{9+}–Sn^{15+} to the spectrum are determined for each experimental condition. The variations of these contributions can be used as a proxy for the charge state populations in the plasma. In

order to understand the scaling of temperature with laser intensity, the fitting results are compared to charge state population calculations performed with the non-equilibrium plasma-population kinetic code FLYCHK. The comparison shows that, for the EUV source here investigated, plasma temperature scales rather weakly with laser intensity, much weaker than expected when looking at theoretical scalings found in previous publications.

The concepts of radiation transport and optical depth, important for every heavily-radiating medium, are introduced in chapter 5. A multitude of experimental EUV spectra were obtained from the droplet-based EUV source at ARCNL, whereby the laser energy, laser pulse duration, and droplet size were varied while maintaining the average laser intensity. Increasing droplet size or laser-pulse duration is shown to broaden the emission spectra, a phenomenon most commonly associated with an increase in the number of absorbers in the plasma. A simple 1D radiation transport model is employed, which, surprisingly, is able to explain all the experimental spectra in terms of an increase of optical depth, the quantity directly related to the column density of Sn ions that affect the emission properties of the plasma. The knowledge of this scaling may drive the improvement of 1-μm-driven EUV sources to compete against 10-μm-driven sources in term of performance.

Chapter 6 deals with the topic of the opacity of Sn laser-produced-plasma. Opacity is closely related to be the absorption spectra of a medium and its characteristics are determined by the elements atomic structure and their level populations. Moreover, in certain equilibrium conditions, opacities are also directly connected to the emission characteristics of a plasma. Overall, these quantities are of great interest for modeling radiation transport in a system such as Sn laser-produced plasma, for example in radiation hydrodynamics simulations. The work in this chapter presents extensive opacity calculations, performed at the Los Alamos National Laboratory, which include 10^{10} electric dipole transitions per ions. The calculations are able to excellently reproduce the experimental spectra measured at ARCNL, highlighting that the vast majority of the light emission originates from transitions between highly-excited states serendipitously aligned around 13.5 nm, and not from singly-excited, 92-eV-average-energy states decaying to the ground configuration. These properties, overlooked in the literature thus far, demonstrate that the common picture of light emission from highly charged tin ions in laser-produced plasma must be revised.